

Analytical Prediction of Electromagnetic Performance of Surface-Mounted Permanent Magnet Machines Based on Subdomain Model Accounting for Tooth-Tips

L. J. Wu¹, Z. Q. Zhu¹, *Fellow, IEEE*, D. Staton², M. Popescu², and D. Hawkins²

¹Department of Electronic and Electrical Engineering, University of Sheffield, Mappin Street, Sheffield S1 3JD, UK

²Motor Design Ltd, 4 Scotland Street, Ellesmere, Shropshire, SY12 0EG, UK

The developed subdomain model accounting for tooth-tips can accurately predict the open-circuit, armature reaction and on-load field distributions in surface-mounted permanent magnet machines. Based on this field model, their electromagnetic performance of the machine, such as the cogging torque, back-EMF and electromagnetic torque, and winding inductances are calculated. The model can also be used for the evaluation of demagnetization withstand capability. The finite element analysis confirms excellent accuracy of the developed analytical model.

Index Terms—Cogging torque, demagnetization withstand capability, electromagnetic torque, inductance, magnetic field, Maxwell stress tensor, slotting effect, subdomain model.

I. INTRODUCTION

ANALYTICAL models remain an important tool for understanding, design and optimisation of surface-mounted permanent magnet machines. These machines excel conventional machines in efficiency, power and torque densities and are increasingly popular in domestic, industrial, and aerospace applications. The objective of this paper is to analytically predict the electromagnetic performance and parameters, such as cogging torque, back-EMF, and electromagnetic torque, inductance, and demagnetization withstand capability of surface-mounted permanent magnet (PM) machines based on a subdomain field model accounting for tooth-tips.

Many papers addressed the subdomain field model for the PM machines [1-6]. Its accuracy was demonstrated to be higher than the permeance model [7, 8] for the cogging torque in [9]. The open-circuit subdomain model neglecting tooth-tips was proposed in [1-6], while the subdomain model for predicting armature reaction field was reported in [10, 11]. However, the influence of tooth-tips is neglected in all these models. Thus, the subdomain model accounting for tooth-tips for open-circuit [12] and armature reaction [13] fields were proposed and its excellent accuracy was demonstrated in literature. In this paper, the load field is solved by the subdomain model accounting for tooth-tips, a combination of models in [12, 13]. The relative permeance of magnets is accurately accounted for. This analytical field model will be used as a basis for predicting the electromagnetic performance and parameters as well as the demagnetization withstand capability.

The popular methods for predicting electromagnetic performance are based on the PM flux linkage, an integral of normal flux density along stator bore considering the coil in the slot as either a punctual current [7, 14-19] or a current sheet over the slot opening [20-22]. But the flux passing through the conductors are neglected or approximate. Thus, the flux linkage will be predicted by an integral of vector potential in the conductor area in this paper. The back-EMF

and electromagnetic torque will be calculated from the obtained flux linkage. The flux passing through the conductors can be accurately accounted for by this method.

The major advantage of the subdomain model accounting for tooth-tips is its accurate field prediction in both the air-gap and slot [13]. Hence a good example of its application is the prediction of winding inductance, of which a large portion may be the slot leakage inductance in the PM machines [23]. The classic 1-D models for the air-gap inductance calculation of the conventional machines [24-26] are not suitable for the permanent magnet machines due to relatively large effective air-gap length in PM machines [23, 27]. A 2-D model was reported in [27] but was developed for slotless machines. The 2-D models for slotted machines to date [28-30] usually treated the winding as a current sheet over slot opening and thus the slotting effect was approximate. As for the slot leakage inductances, the classic 1-D models [26, 30] are adequate for the conventional machines which usually have deep and narrow slots, but may not be appropriate for permanent magnet machines. Different from the conventional machines, the non-overlapping winding, i.e. two sides of coils are housed in one slot circumferentially side-by-side, finds popular applications but results in the asymmetrical field distribution in the PM machines [23]. The less number of slots in the non-overlapping fractional-slot machines also makes the slot width comparable to slot depth. A 2-D model for the slot leakage inductances was proposed in [23], which can deal with the non-overlapping winding distribution. The application of subdomain model to the inductance prediction can be found in [11] considering both non-overlapping and overlapping windings. Although the 2-D field distribution can be predicted by the subdomain model in both slot and air-gap, the inductance is calculated from a line integral of flux density along certain path either radially in the middle of slot for the slot leakage inductances or on the stator bore for the air-gap inductances. However, the complicated flux linkage in the slot and slot opening cannot be simply dealt with by a line integral of flux density. In addition, the tooth-tips are neglected and hence it is suitable for only open slot machines. In this paper,

$$M_{rk} = (B_r / \mu_0) \alpha_p (A_{1k} + A_{2k}) \quad k/p = 1, 3, 5, \dots \quad (12)$$

$$M_{\alpha k} = (B_r / \mu_0) \alpha_p (A_{1k} - A_{2k}) \quad k/p = 1, 3, 5, \dots \quad (13)$$

where

$$A_{1k} = \frac{\sin[(k+1)\alpha_p(\pi/2/p)]}{(k+1)\alpha_p(\pi/2/p)} \quad (14)$$

$$A_{2k} = \frac{\sin[(k-1)\alpha_p(\pi/2/p)]}{(k-1)\alpha_p(\pi/2/p)} \quad (15)$$

where B_r is the residual flux density of magnet and α_p is the pole arc to pitch ratio, ω_r is the rotor rotational speed, α_0 is the rotor initial position, p is the number of pole pairs.

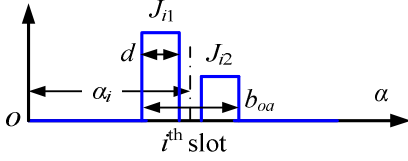


Fig. 3. Current density function of non-overlapping winding.

The current density J as shown in Fig. 3 can be expressed by:

$$J = J_{i0} + \sum_n J_{in} \cos[E_n(\alpha + b_{sa}/2 - \alpha_i)] \quad (16)$$

for $\alpha_i - b_{sa}/2 \leq \alpha \leq \alpha_i + b_{sa}/2$, where α_i is the slot position, b_{sa} is the slot width angle as shown in Fig. 2(b),

$$J_{i0} = (J_{i1} + J_{i2})d / b_{oa} \quad (17)$$

$$J_{in} = \frac{2}{n\pi} (J_{i1} + J_{i2} \cos n\pi) \sin(n\pi d / b_{oa}) \quad (18)$$

$$E_n = n\pi / b_{sa} \quad (19)$$

Considering the boundary condition along the rotor yoke, the vector potential in the magnets can be expressed by:

$$A_{z1} = \sum_k (C_{1k} A_1 + C_{2k} M_{\alpha ck} - C_{3k} M_{rsk}) \cos(k\alpha) + \sum_k (C_{1k} C_1 + C_{2k} M_{\alpha sk} + C_{3k} M_{rck}) \sin(k\alpha) \quad (20)$$

where

$$C_{1k} = \left[(r/R_m)^k + G_1 (r/R_r)^{-k} \right] \quad (21)$$

$$C_{2k} = \frac{\mu_0}{k^2 - 1} \left[R_r k (r/R_r)^{-k} + r \right] \quad (22)$$

$$C_{3k} = \frac{\mu_0}{k^2 - 1} \left[R_r (r/R_r)^{-k} + kr \right] \quad (23)$$

$$G_1 = (R_r / R_m)^k \quad (24)$$

The general solution of vector field in the air-gap is:

$$A_{z2} = \sum_k \left[A_2 (r/R_s)^k + B_2 (r/R_m)^{-k} \right] \cos(k\alpha) + \sum_k \left[C_2 (r/R_s)^k + D_2 (r/R_m)^{-k} \right] \sin(k\alpha) \quad (25)$$

where R_s is the radius of stator bore.

Considering the boundary condition along the bottom and both sides of the slot, the vector potential distribution in the slot of the non-overlapping winding machine can be derived as:

$$A_{z3i} = A_0 + \sum_n A_n \cos[E_n(\alpha + b_{sa}/2 - \alpha_i)] \quad (26)$$

where

$$A_0 = \mu_0 J_{i0} (2R_{sb}^2 \ln r - r^2) / 4 + Q_{3i} \quad (27)$$

$$A_n = D_{3i} \left[G_3 (r/R_{fb})^{E_n} + (r/R_t)^{-E_n} \right] + \mu_0 \frac{J_{in}}{E_n^2 - 4} \left[r^2 - \frac{2}{E_n} R_{sb}^2 (r/R_{sb})^{E_n} \right] \quad (28)$$

where R_{fb} and R_t are the radii of the bottom and top of slot, respectively, and

$$G_3 = (R_t / R_{sb})^{E_n} \quad (29)$$

For overlapping winding machine, the vector potential distribution in the slot can be given by:

$$A_{z3} = A_{bi0} + \sum_n A_{bin} \cos[E_n(\alpha + b_{sa}/2 - \alpha_i)] \quad (30)$$

for the bottom part of the slot and

$$A_{z3} = A_{ti0} + \sum_n A_{tin} \cos[E_n(\alpha + b_{sa}/2 - \alpha_i)] \quad (31)$$

for the top part of the slot, where

$$A_{bi0} = \mu_0 J_{i2} (2R_{sb}^2 \ln r - r^2) / 4 + Q_{3bi} \quad (32)$$

$$A_{ti0} = \mu_0 J_{i1} (R_{sm}^2 \ln r - r^2) / 2 + \mu_0 J_{i2} (R_{sb}^2 - R_{sm}^2) \ln(r) / 2 + Q_{3ti} \quad (33)$$

$$A_{bin} = A_{tin} = D_{3i} \left[G_3 (r/R_{sb})^{E_n} + (r/R_t)^{-E_n} \right] \quad (34)$$

Satisfying the boundary condition on both sides of the slot opening, the general solution of vector field in the i th slot opening can be given by:

$$A_{z4i} = D \ln r + Q_{4i} + \sum_m \left[C_{4i} \left(\frac{r}{R_t} \right)^{F_m} + D_{4i} \left(\frac{r}{R_s} \right)^{-F_m} \right] \cos \left[F_m \left(\alpha + \frac{b_{oa}}{2} - \alpha_i \right) \right] \quad (35)$$

where b_{oa} is the slot opening width angle as shown in Fig. 1(b), D is constant, and

$$F_m = m\pi / b_{oa} \quad (36)$$

The unknown coefficients A_2 , B_2 , C_2 , D_2 , C_{3i} , D_{3i} , Q_{3i} , C_{4i} , D_{4i} , Q_{4i} and D in the expressions of vector potentials can be determined by applying the interface conditions between subdomains, viz. the continuations of normal flux density and tangential vector potential across the interface. The detail calculation method is given in the appendix.

2) Flux Density

The radial and circumferential components of flux density can be obtained from the vector potential distribution by:

$$B_r = \frac{1}{r} \frac{\partial A_z}{\partial \alpha} \quad \text{and} \quad B_\alpha = -\frac{\partial A_z}{\partial r} \quad (37)$$

The magnetic intensity can be obtained by:

$$B = \mu_0 \mu_r H + \mu_0 M \quad (38)$$

in the magnet and

$$B = \mu_0 H \quad (39)$$

in the air-gap, slot opening and slot.

Therefore, the flux density in the magnet can be given by:

$$B_{1r} = -(1/r) \sum_k k (C_{1k} A_1 + C_{2k} M_{\alpha ck} - C_{3k} M_{rsk}) \sin(k\alpha) + (1/r) \sum_k k (C_{1k} C_1 + C_{2k} M_{\alpha sk} + C_{3k} M_{rck}) \cos(k\alpha) \quad (40)$$

for the radial component and

$$B_{1\alpha} = -(1/r) \sum_k (C_{4k} A_1 + C_{5k} M_{\alpha ck} - C_{6k} M_{rsk}) \cos(k\alpha) \\ - (1/r) \sum_k (C_{4k} C_1 + C_{5k} M_{\alpha sk} + C_{6k} M_{rck}) \sin(k\alpha) \quad (41)$$

for the circumferential component, where

$$C_{4k} = k \left[(r/R_m)^k - G_1 (r/R_r)^{-k} \right] \quad (42)$$

$$C_{5k} = \frac{\mu_0}{k^2 - 1} \left[-k^2 R_r (r/R_r)^{-k} + r \right] \quad (43)$$

$$C_{6k} = \frac{\mu_0 k}{k^2 - 1} \left[-R_r (r/R_r)^{-k} + r \right] \quad (44)$$

The flux density in the air-gap can be given by:

$$B_{2r} = \sum_k B_{rs} \sin(k\alpha) + \sum_k B_{rc} \cos(k\alpha) \quad (45)$$

for the radial component and

$$B_{2\alpha} = \sum_k B_{\alpha c} \cos(k\alpha) + \sum_k B_{\alpha s} \sin(k\alpha) \quad (46)$$

where

$$B_{rs} = -k \left[A_2 (r/R_s)^k + B_2 (r/R_m)^{-k} \right] / r \quad (47)$$

$$B_{rc} = k \left[C_2 (r/R_s)^k + D_2 (r/R_m)^{-k} \right] / r \quad (48)$$

$$B_{\alpha c} = -k \left[A_2 (r/R_s)^k - B_2 (r/R_m)^{-k} \right] / r \quad (49)$$

$$B_{\alpha s} = -k \left[C_2 (r/R_s)^k - D_2 (r/R_m)^{-k} \right] / r \quad (50)$$

As for the non-overlapping winding, the flux density in the i th slot can be expressed as:

$$B_{3ir} = -\sum_n \frac{E_n D_{3i}}{r} \left[G_3 (r/R_{sb})^{E_n} + (r/R_t)^{-E_n} \right] \\ \cdot \sin \left[E_n (\alpha + b_{sa} / 2 - \alpha_i) \right] - \mu_0 \sum_n \frac{J_{in}}{E_n^2 - 4} \\ \cdot \left[E_n r - 2R_{sb} (r/R_{sb})^{E_n - 1} \right] \sin \left[E_n (\alpha + b_{sa} / 2 - \alpha_i) \right] \quad (51)$$

for the radial component and

$$B_{3i\alpha} = -\mu_0 J_{i0} (R_{sb}^2 - r^2) / (2r) \\ - \sum_n \frac{E_n D_{3i}}{r} \left[G_3 (r/R_{sb})^{E_n} - (r/R_t)^{-E_n} \right] \cos \left[E_n \left(\alpha + \frac{b_{sa}}{2} - \alpha_i \right) \right] \\ - 2\mu_0 \sum_n \frac{J_{in}}{E_n^2 - 4} \left[r - R_{sb} (r/R_{sb})^{E_n - 1} \right] \cos \left[E_n \left(\alpha + \frac{b_{sa}}{2} - \alpha_i \right) \right] \quad (52)$$

for the circumferential component.

As for the overlapping winding, the radial component flux density in the slot can be given as:

$$B_{3ir} = -\sum_n \frac{E_n D_{3i}}{r} \left[G_3 (r/R_{sb})^{E_n} + (r/R_t)^{-E_n} \right] \\ \cdot \sin \left[E_n (\alpha + b_{sa} / 2 - \alpha_i) \right] \quad (53)$$

and the circumferential component flux density in the slot can be expressed by:

$$B_{3i\alpha} = -\sum_n \frac{E_n D_{3i}}{r} \left[G_3 (r/R_{sb})^{E_n} - (r/R_t)^{-E_n} \right] \\ \cdot \cos \left[E_n (\alpha + b_{sa} / 2 - \alpha_i) \right] - \mu_0 J_{i2} (R_{sb}^2 - r^2) / (2r) \quad (54)$$

in the bottom part of slot and

$$B_{3i\alpha} = -\mu_0 \left[J_{i1} (R_{sm}^2 - r^2) + J_{i2} (R_{sb}^2 - R_{sm}^2) \right] / (2r) \\ - (1/r) \sum_n E_n D_{3i} \left[G_3 (r/R_{sb})^{E_n} - (r/R_t)^{-E_n} \right] \\ \cdot \cos \left[E_n (\alpha + b_{sa} / 2 - \alpha_i) \right] \quad (55)$$

in the top part of slot.

The flux density in the i th slot opening can be expressed as:

$$B_{4ir} = -(1/r) \sum_m F_m \left[C_{4i} (r/R_t)^{F_m} + D_{4i} (r/R_s)^{-F_m} \right] \\ \cdot \sin \left[F_m (\alpha + b_{oa} / 2 - \alpha_i) \right] \quad (56)$$

for the radial component and

$$B_{4i\alpha} = -(1/r) \sum_m F_m \left[C_{4i} (r/R_t)^{F_m} - D_{4i} (r/R_s)^{-F_m} \right] \\ \cdot \cos \left[F_m (\alpha + b_{oa} / 2 - \alpha_i) \right] - D / r \quad (57)$$

for the circumferential component.

III. ELECTROMAGNETIC PERFORMANCE

1) Back-EMF and Torque

A. For Non-Overlapping Winding

The flux linkage with one coil side as shown in Fig. 2(a) can be calculated from the vector potential distribution [32]:

$$\psi_{i1} = l_a \frac{N_c}{A_c} \int_{R_t}^{R_{sb}} \int_{\alpha_i - b_{sa}/2}^{\alpha_i - b_{sa}/2 + d} A_{z3i} r dr d\alpha \\ = l_a (N_c / A_c) \left[Z_0 d + \sum_n (Z_n / E_n) \sin(E_n d) \right] \quad (58)$$

where l_a is the active length, N_c is the number of turns per coil, A_c is the area of one coil side, d is the circumferential width of the coil side, and

$$Z_0 = \int_{R_t}^{R_{sb}} A_0 r dr \\ = Q_{3i} (R_{sb}^2 - R_t^2) / 2 + \mu_0 J_{i0} \\ \cdot (4R_{sb}^4 \ln R_{sb} - 4R_{sb}^2 R_t^2 \ln R_t - 3R_{sb}^4 + 2R_{sb}^2 R_t^2 + R_t^4) / 16 \quad (59)$$

$$Z_n = \int_{R_t}^{R_{sb}} A_n r dr \\ = \frac{D_{3i} G_3}{2 + E_n} (R_{sb}^2 - R_t^2 G_3) + \frac{D_{3i}}{2 - E_n} (R_{sb}^2 G_3 - R_t^2) \\ + \frac{1}{4} \frac{\mu_0 J_{in}}{E_n^2 - 4} (R_{sb}^4 - R_t^4) + \frac{2\mu_0 J_{in} R_{sb}^2}{E_n (E_n^2 - 4) (E_n + 2)} (R_t^2 G_3 - R_{sb}^2) \quad (60)$$

Similarly, the flux linkage with another coil side in the slot is:

$$\psi_{i2} = l_a (N_c / A_c) \left[Z_0 d - \sum_n (Z_n / E_n) \sin(n\pi - E_n d) \right] \quad (61)$$

B. For Overlapping Winding

The flux linkage with one coil side as shown in Fig. 2(a) can be calculated from the vector potential distribution [32]:

$$\psi_{i1} = l_a \frac{N_c}{A_c} \int_{R_t}^{R_{sm}} \int_{\alpha_i - b_{sa}/2}^{\alpha_i + b_{sa}/2} A_{z3} r dr d\alpha \\ = l_a (N_c / A_c) Z_{i0} b_{sa} \quad (62)$$

where

$$\begin{aligned} Z_{i0} &= \int_{R_i}^{R_{sm}} A_{i0} r dr \\ &= Q_{3i} (R_{sm}^2 - R_i^2) / 2 + \\ &\mu_0 J_{i2} (R_{sb}^2 - R_{sm}^2) [R_{sm}^2 (2 \ln R_{sm} - 1) - R_i^2 (2 \ln R_i - 1)] / 8 + \\ &\mu_0 J_{i1} (4R_{sm}^4 \ln R_{sm} - 4R_{sm}^2 R_i^2 \ln R_i - 3R_{sm}^4 + 2R_{sm}^2 R_i^2 + R_i^4) / 16 \end{aligned} \quad (63)$$

Similarly, the flux linkage with another coil side in the slot is:

$$\psi_{i2} = l_a (N_c / A_c) Z_{b0} b_{sa} \quad (64)$$

where

$$\begin{aligned} Z_{b0} &= \int_{R_{sm}}^{R_{sb}} A_{b0} r dr \\ &= Q_{3bi} (R_{sb}^2 - R_{sm}^2) / 2 + \mu_0 J_{i2} \\ &\cdot (4R_{sb}^4 \ln R_{sb} - 4R_{sb}^2 R_{sm}^2 \ln R_{sm} - 3R_{sb}^4 + 2R_{sb}^2 R_{sm}^2 + R_{sm}^4) / 16 \end{aligned} \quad (65)$$

It should be noted that J_{i0} , J_{in} , J_{i1} , and J_{i2} are included in (59), (60), (63) and (65) for the calculation of inductance in the next section, but are zero for the calculation of open-circuit flux linkage.

The total flux linkage of each phase can be obtained by summing the flux linkages associated with all coil sides of the corresponding phase. Then, the back-EMF is calculated by the derivative of the flux linkage with respect to time when the winding is open-circuit.

The electromagnetic torque can be obtained from the back-EMF by:

$$T_{em} = (E_A I_A + E_B I_B + E_C I_C) / \omega_r \quad (66)$$

As for the cogging torque, the calculation should be based on the open-circuit field. Many methods were proposed, such as the energy [33, 34], lateral force [35], and complex permeance [7, 8]. However, benefiting from the excellent accuracy in the airgap field prediction by the subdomain model accounting for tooth-tips, the Maxwell stress tensor is employed in this paper to calculate the cogging torque based on the open-circuit field distribution [5]:

$$\begin{aligned} T_c &= (l_a r^2 / \mu_0) \int_0^{2\pi} B_{2r} B_{2\alpha} d\alpha \\ &= (\pi l_a r^2 / \mu_0) \sum_k (B_{rck} B_{\alpha ck} + B_{rsk} B_{\alpha sk}) \end{aligned} \quad (67)$$

Equation (67) can also be used for predicting the total torque including both cogging and electromagnetic torques if the open-circuit flux density is substituted by the on-load flux density.

2) Inductances

The self- and mutual-inductances can be calculated from the energy [23, 27]:

$$L = 2W_A / I_A^2 \quad (68)$$

$$M = (W_{AB} - W_A - W_B) / (I_A I_B) \quad (69)$$

where W_A , W_B , and W_{AB} are the magnetic energies when the magnets are not magnetized and the machine is fed with I_A only, I_B only, and both I_A and I_B , respectively.

The energy can be obtained by [23, 27]:

$$W = (l_a / 2) \sum_i \int_{R_i}^{R_m} \int_{\alpha_i - b_{sa}/2}^{\alpha_i + b_{sa}/2} A J r d\alpha dr \quad (70)$$

For the non-overlapping winding:

$$W = l_a b_{sa} \sum_i Z_{i0} J_{i0} / 2 + l_a b_{sa} \sum_i \sum_n Z_n J_{in} / 4 \quad (71)$$

and for the overlapping winding:

$$W = l_a b_{sa} \sum_i Z_{b0} J_{i2} / 2 + l_a b_{sa} \sum_i Z_{i0} J_{i1} / 2 \quad (72)$$

3) Evaluation of Demagnetization Withstand Capability

One of advantages of the developed model is that it can be used to evaluate the demagnetization withstand capability accounting for the stator slotting effect. To assess the risk of the partial irreversible demagnetization, the flux density distribution along the magnet surface needs to be evaluated for every rotor positions.

For uniform distributed magnets, it is enough evaluate only one magnet. The criterion to avoid partial irreversible demagnetization is within an electrical period:

$$D_{mg} \cdot B_{lr} \Big|_{r \rightarrow R_m} > B_d \quad (73)$$

for the radial magnetization, and

$$D_{mg} \left[B_{lr} \cos(\alpha - \alpha_{mg}) - B_{l\alpha} \sin(\alpha - \alpha_{mg}) \right] \Big|_{r \rightarrow R_m} > B_d \quad (74)$$

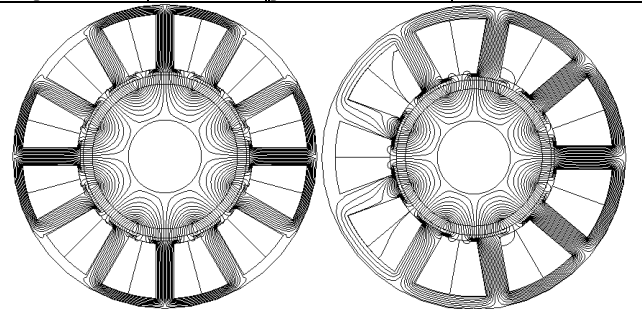
for the parallel magnetization, where D_{mg} is equal to 1 or -1 for the outward and inward magnetization, respectively, α_{mg} is the position of the magnet to be evaluated and B_d is the minimum flux density of magnet for safe operation at a specific temperature.

IV. FINITE ELEMENT VALIDATION AND INVESTIGATION

The finite element analysis is carried out to validate the analytical prediction on three machines. Their main parameters are shown in Table I and the equal potential distributions when the machines are either open-circuit or fed with only I_a are shown in Fig. 4 and Fig. 5, respectively.

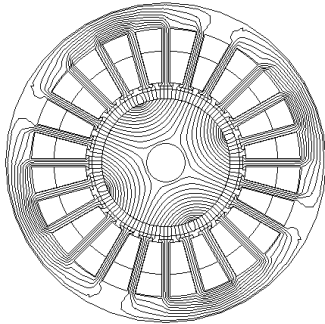
Table I
MAIN PARAMETERS OF MACHINES (Default Unit: mm)

Machine	I-III	Machine	I	II	III
Pole number/slot number	8p/12s, 8p/9s, 4p/24s	Pole number/slot number	8p/12s	8p/9s	4p/24s
Rated speed	400 (rpm)	Tooth tip edge	1	1	1
Stator outer diameter	100	Stator inner diameter	55.7	53	48
Air-gap length	1	Rotor outer diameter	53.7	51	46
Axial length	50	Stator yoke height	3.2	4.4	8.1
Magnet thickness	3	Winding turns/phase	136	132	104
Magnet μ_r	1.05	Coil pitch	1	1	5
Remanence	1.2 (T)	Rated current	10 (A_{peak})		
Slot-opening to slot-pitch ratio	0.3	Slot-width to slot-pitch ratio	0.6		



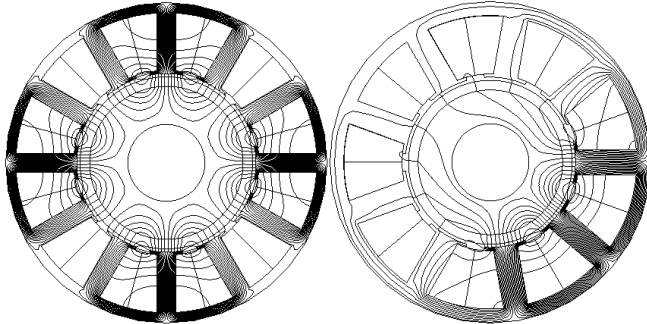
(a) 8-pole/12-slot

(b) 8-pole/9-slot



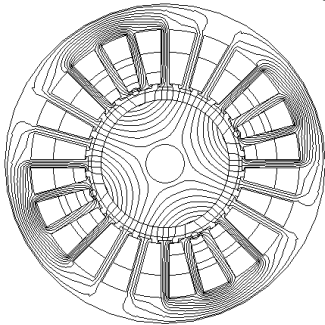
(c) 4-pole/24-slot

Fig. 4. Open-circuit equal potential distributions.



(a) 8-pole/12-slot

(b) 8-pole/9-slot

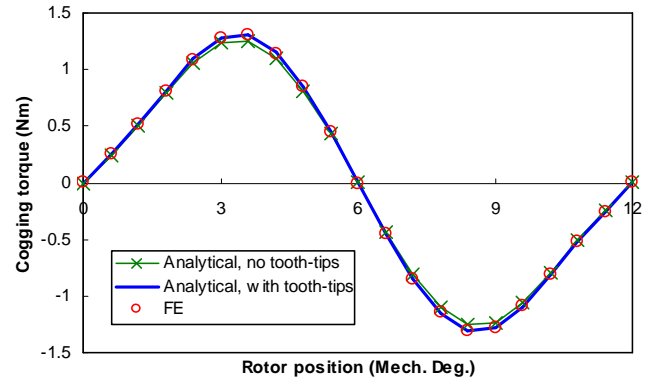


(c) 4-pole/24-slot

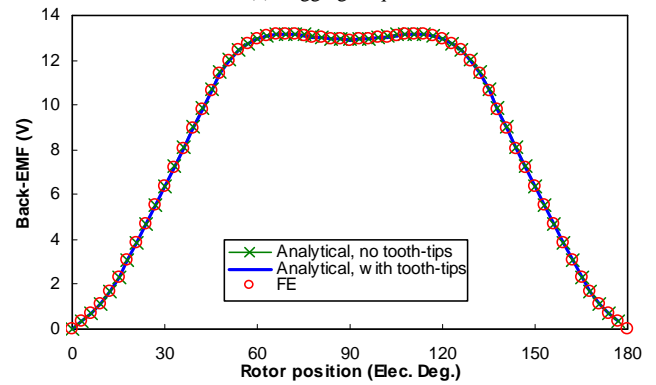
Fig. 5. Equal potential distributions of armature reaction fields, $I_a=10A$, $I_b=I_c=0$.

A. Back-EMF and Torque

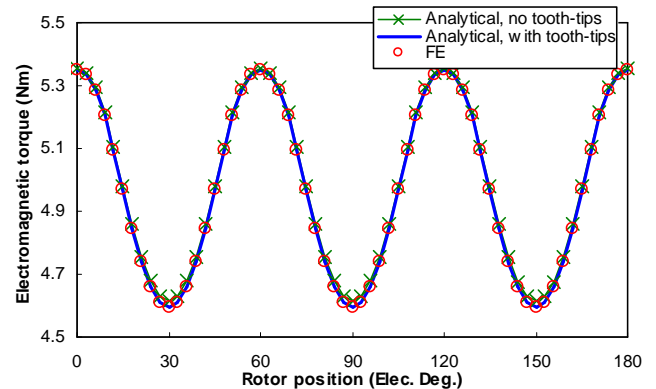
Fig. 6 and Fig. 7 show the comparison between analytically and FE predicted back-EMF and electromagnetic torque waveforms of the 8-pole/12-slot and 8-pole/9-slot machines, respectively. All analytical models show a good agreement with FE. The difference between the predictions based on the subdomain models with/without accounting for tooth-tips is negligible for back-EMF and electromagnetic torque, since the influence of tooth-tips on the air-gap flux density distribution is small [12, 13]. But as the cogging torque is more sensitive, the neglect of tooth-tips shows relative large error in the cogging torque of the 8-pole/9-slot machine.



(a) Cogging torque

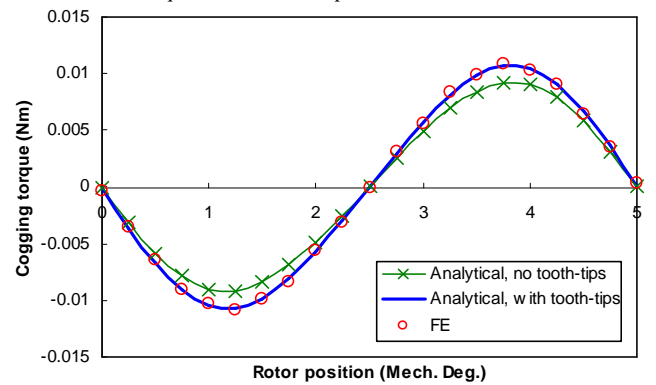


(b) Phase back-EMF



(c) Electromagnetic torque

Fig. 6. Analytically and FE predicted back-EMF, cogging and electromagnetic torque waveforms of 8-pole/12-slot machine.



(a) Cogging torque

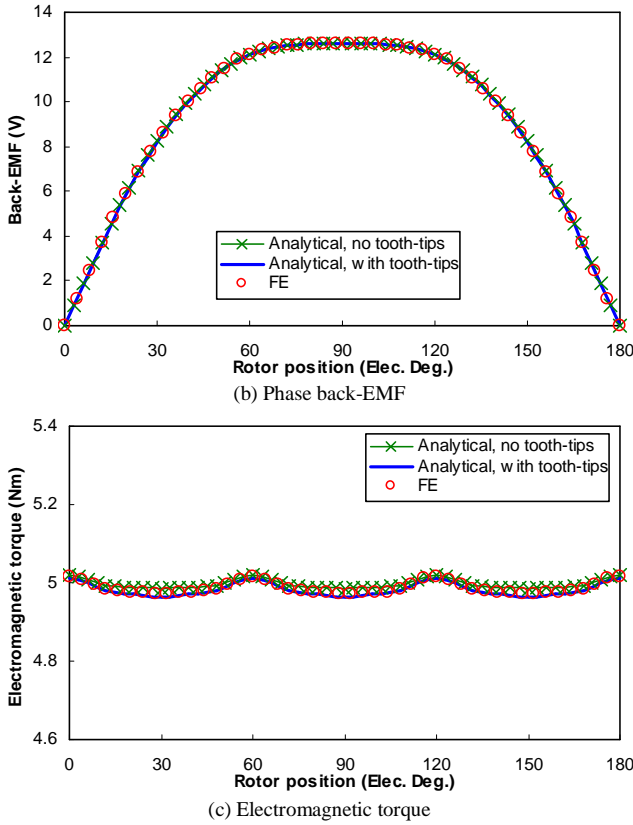


Fig. 7. Analytically and FE predicted back-EMF, cogging and electromagnetic torque waveforms of 8-pole/9-slot machine.

Fig. 8 shows the analytically predicted variation of average torque with the winding coil width d in the 8-pole/12-slot machine when all other parameters are kept same. But generally, the influence of coil width on the average torque is small. The influence can be noticeable only for the large slot-opening to slot-depth ratio.

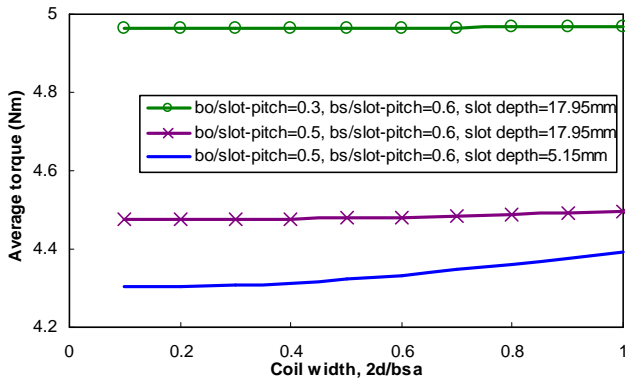


Fig. 8. Analytically predicted variation of average torque with coil width.

B. Inductances

The analytical and FE predicted self- and mutual-inductances are compared in Table II. The excellent agreement between the predictions of both self- and mutual-inductances by FE and the analytical model considering the tooth-tips shows its much better accuracy than the model neglecting the tooth-tips.

Table II
SELF- AND MUTUAL-INDUCTANCES

Machine (Pole number/slot number)	8p/12s	8p/9s	4p/24s	
Self-inductance, mH	Analytical, no tooth-tips	1.53	2.80	2.04
	Analytical, with tooth-tips	1.31	2.49	1.72
	FE	1.29	2.51	1.69
Mutual-inductance, mH	Analytical, no tooth-tips	-0.75	-0.19	-0.62
	Analytical, with tooth-tips	-0.62	-0.15	-0.58
	FE	-0.6	-0.15	-0.57

The variation of self- and mutual inductances with the slot opening width is studied by the analytical models considering/neglecting tooth-tips and the results are shown in Fig. 9. The difference between them increases with the difference between the slot opening width b_o and slot width b_s . Both self- and mutual-inductances can be significantly overestimated by the model neglecting tooth-tips for the machine having a relative small slot opening width b_o with respect to its slot width b_s .

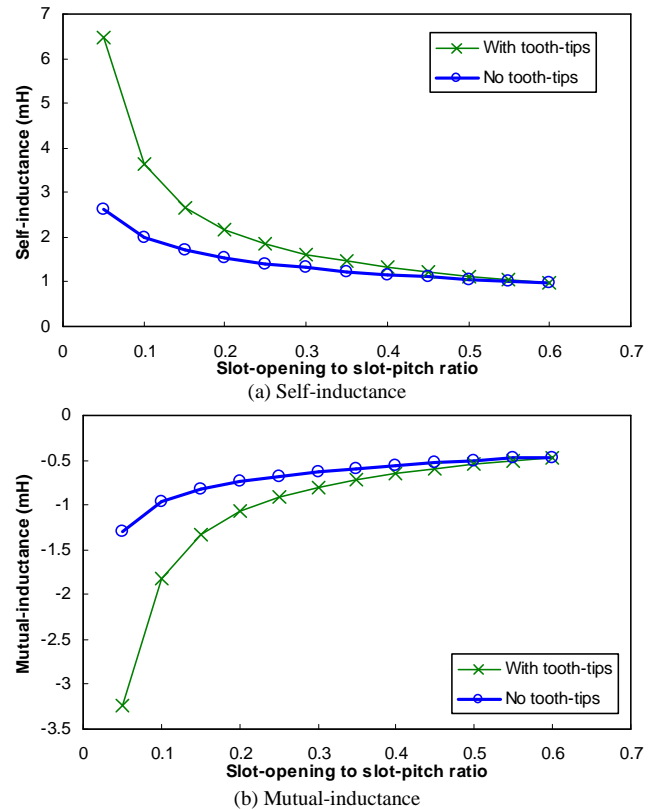


Fig. 9. Analytically predicted variation of inductances with slot-opening of 8-pole/12-slot machine.

C. Demagnetization Withstand Capability

The demagnetization withstand capability of the 8-pole/12-slot machine is evaluated under 60°C and 80°C. By way of example, $B_r=1.14\text{T}$ and $B_d=0.3\text{T}$ at 60°C and $B_r=1.11\text{T}$ and $B_d=0.46\text{T}$ at 80°C, for a moderate cost N35 magnet material.

Fig. 10 shows the comparison between the on-load flux density predictions on the surface of magnets by the analytical model and FE. The excellent agreement verifies the capability of the analytical model as an assessment tool of the irreversible demagnetization risk.

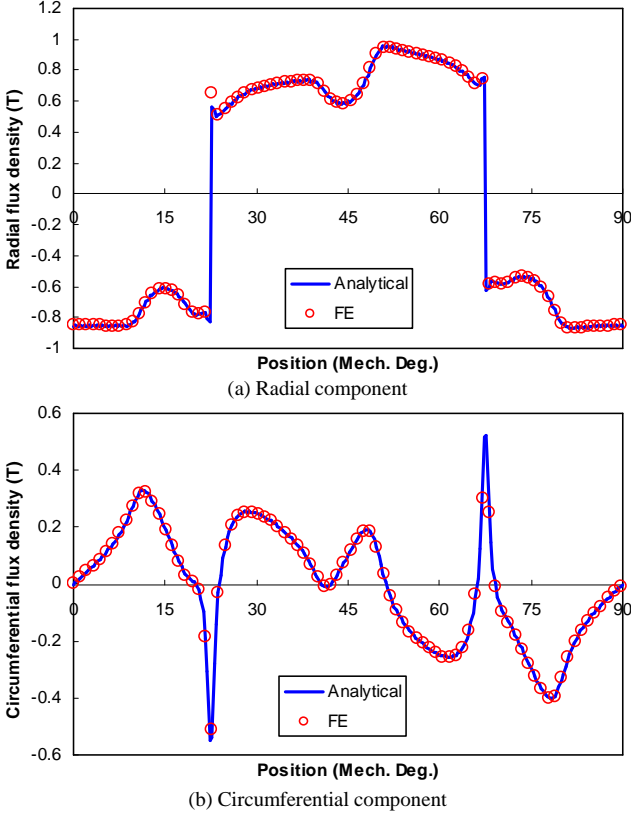


Fig. 10. Analytically and FE predicted flux density waveforms in magnets of 8-pole/12-slot machine, $B_r=1.11\text{T}$, $r=R_m-0.1\text{mm}$.

Fig. 11 shows the minimum flux densities in the direction of magnetization at different positions on the magnet surface during the whole operation cycle. It shows that it is safe when the machine is operated at 60°C , but the partial irreversible demagnetization occurs at the tailing edge of the magnet if magnet temperature is 80°C .

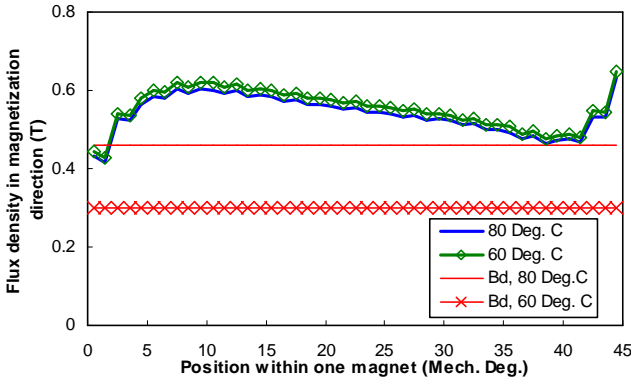


Fig. 11. Analytically predicted minimum flux density on the magnet surface during operation of 8-pole/12-slot machine at 60°C and 80°C .

V. CONCLUSIONS

The developed subdomain model accounting for tooth-tips can accurately predict the open-circuit, armature reaction and on-load field distributions in surface-mounted permanent magnet machines. Based on this field model, the electromagnetic performances of the machine, such as the cogging torque, back-EMF, electromagnetic torque, and inductances, can be accurately calculated. The model can also

be used for the evaluation of demagnetization withstand capability. The FE analysis confirms the excellent accuracy of the analytical model.

APPENDIX

The flux density and vector potential along the interface between Regions I and II should satisfy:

$$B_{I\alpha} = B_{II\alpha} \quad \text{and} \quad A_I = A_{II} \quad (75)$$

C. Interface between Permanent Magnet and Air-gap

Because the normal flux density is continuous between magnet and air-gap, the following expressions can be obtained:

$$A_2 G_2 + B_2 = A_1 (1 + G_1^2) + \mu_0 [(R_r k G_1 + R_m) M_{\alpha ck} - (R_r G_1 + k R_m) M_{rsk}] / (k^2 - 1) \quad (76)$$

$$C_2 G_2 + D_2 = C_1 (1 + G_1^2) + \mu_0 [(R_r k G_1 + R_m) M_{\alpha sk} + (R_r G_1 + k R_m) M_{rck}] / (k^2 - 1) \quad (77)$$

where

$$G_2 = (R_m / R_s)^k \quad (78)$$

The circumferential magnetic field intensity is continuous between magnet and air-gap, and hence the following equations can be obtained:

$$\mu_r (A_2 G_2 - B_2) = A_1 (1 - G_1^2) + \mu_0 [k (R_m - R_r G_1) M_{\alpha ck} - (R_m - R_r G_1) M_{rsk}] / (k^2 - 1) \quad (79)$$

$$\mu_r (C_2 G_2 - D_2) = C_1 (1 - G_1^2) + \mu_0 [k (R_m - R_r G_1) M_{\alpha sk} + (R_m - R_r G_1) M_{rck}] / (k^2 - 1) \quad (80)$$

D. Interface between Slot Opening and Slot

The circumferential component of the flux density along the interface between slot and slot opening can be obtained as:

$$B_{4i\alpha} \Big|_{r=R_t} = B_{4i\alpha 0} + \sum_m B_{4i\alpha m} \cos [F_m (\alpha + b_{oa} / 2 - \alpha_i)] \quad (81)$$

where

$$B_{4i\alpha 0} = -D / R_t \quad (82)$$

$$B_{4i\alpha m} = -F_m (C_{4i} - D_{4i} G_4) / R_t \quad (83)$$

$$G_4 = (R_s / R_t)^{F_m} \quad (84)$$

The circumferential component of the flux density in the slot along the radius R_t outside the slot opening region is zero since the stator core material is infinitely permeable. The circumferential component of the flux density along the radius R_t can be expanded into Fourier series over $[\alpha_r - b_{sa} / 2, \alpha_r + b_{sa} / 2]$:

$$B_{4i\alpha} \Big|_{r=R_t} = B_0 + \sum_n B_n \cos [E_n (\alpha + b_{sa} / 2 - \alpha_i)] \quad (85)$$

where

$$B_0 = B_{4i\alpha 0} \gamma_a \quad (86)$$

$$B_n = B_{4i\alpha 0} \gamma_0 + \sum_m B_{4i\alpha m} \gamma \quad (87)$$

where

$$\gamma_a = b_{oa} / b_{sa} \quad (88)$$

$$\gamma_0(n) = 4 \cos(n\pi/2) \sin(E_n b_{oa}/2) / (n\pi) \quad (89)$$

$$\gamma(m, n) = -\frac{2}{b_{sa}} \frac{E_n}{F_m^2 - E_n^2} \left[\cos(m\pi) \sin\left(E_n \frac{b_{sa} + b_{oa}}{2}\right) - \sin\left(E_n \frac{b_{sa} - b_{oa}}{2}\right) \right] \quad (90)$$

The circumferential component of the flux density along the interface between slot and slot opening can also be given as:

$$B_{3i\alpha} \Big|_{r=R_i} = B_{3i\alpha 0} + \sum_n B_{3i\alpha n} \cos[E_n(\alpha + b_{sa}/2 - \alpha_i)] \quad (91)$$

where for the non-overlapping winding:

$$B_{3i\alpha 0} = -\mu_0 J_{i0} (R_{sb}^2 - R_i^2) / (2R_i) \quad (92)$$

$$B_{3i\alpha n} = -\frac{1}{R_i} E_n D_{3i} (G_3^2 - 1) - \frac{2\mu_0}{R_i} \frac{J_{in}}{E_n^2 - 4} (R_i^2 - R_{sb}^2 G_3) \quad (93)$$

and for the overlapping winding:

$$B_{3i\alpha 0} = -\mu_0 \left[J_{i1} (R_{sm}^2 - R_i^2) - J_{i2} (R_{sb}^2 - R_{sm}^2) \right] / (2R_i) \quad (94)$$

$$B_{3i\alpha n} = -E_n D_{3i} (G_3^2 - 1) / R_i \quad (95)$$

Applying the interface condition $B_{3i\alpha}|_{r=R_i} = B_{4i\alpha}|_{r=R_i}$ the following equations can be obtained:

$$B_{3i\alpha 0} = B_{4i\alpha 0} \gamma_a \quad (96)$$

$$B_{3i\alpha n} = B_{4i\alpha 0} \gamma_0 + \sum_m B_{4i\alpha m} \gamma \quad (97)$$

According to (96), for the non-overlapping winding:

$$D = \mu_0 J_{i0} (b_{sa} / b_{oa}) (R_{sb}^2 - R_i^2) / 2 \quad (98)$$

and for the overlapping winding:

$$D = \mu_0 (b_{sa} / b_{oa}) \left[J_{i1} (R_{sm}^2 - R_i^2) + J_{i2} (R_{sb}^2 - R_{sm}^2) \right] / 2 \quad (99)$$

The vector potential distribution in Region 3i along the radius R_i can be given by:

$$A_i = A_{z3i} \Big|_{r=R_i} = A_{3i0} + \sum_n A_{3in} \left[E_n (\alpha + b_{sa} / 2 - \alpha_i) \right] \quad (100)$$

where for the non-overlapping winding:

$$A_{3i0} = \mu_0 J_{i0} (2R_{sb}^2 \ln R_i - R_i^2) / 4 + Q_{3i} \quad (101)$$

$$A_{3in} = D_{3i} (G_3^2 + 1) + \mu_0 \frac{J_{in}}{E_n^2 - 4} (R_i^2 - 2R_{sb}^2 G_3 / E_n) \quad (102)$$

and for the overlapping winding:

$$A_{3i0} = Q_{3i} + \mu_0 \left[J_{i1} (R_{sm}^2 \ln R_i - R_i^2 / 2) + J_{i2} (R_{sb}^2 - R_{sm}^2) \ln R_i \right] / 2 \quad (103)$$

$$A_{3in} = D_{3i} (G_3^2 + 1) \quad (104)$$

A_i can be expanded into Fourier series over the slot opening, viz. $[\alpha_i - b_{oa}/2, \alpha_i + b_{oa}/2]$:

$$A_i = A_{3i0} + \sum_m A_{3im} \cos[F_m(\alpha + b_{oa}/2 - \alpha_i)] \quad (105)$$

for $\alpha_i - b_{oa}/2 \leq \alpha \leq \alpha_i + b_{oa}/2$, where

$$A_{3i0} = \sum_n A_{3in} \zeta_0 + \mu_0 J_{i0} (2R_{sb}^2 \ln R_i - R_i^2) / 4 + Q_{3i} \quad (106)$$

for the non-overlapping winding and

$$A_{3i0} = \sum_n A_{3in} \zeta_0 + Q_{3i} + \mu_0 \left[J_{i1} (R_{sm}^2 \ln R_i - R_i^2 / 2) + J_{i2} (R_{sb}^2 - R_{sm}^2) \ln R_i \right] / 2 \quad (107)$$

for the overlapping winding, and

$$A_{3im} = \sum_n A_{3in} \zeta \quad (108)$$

where

$$\zeta_0(n) = (b_{sa} / b_{oa} / 2) \gamma_0(n) \quad (109)$$

$$\zeta(m, n) = (b_{sa} / b_{oa}) \gamma(m, n) \quad (110)$$

The vector potential distribution along the radius R_i within the slot opening can also be expressed by:

$$A_{z4i} \Big|_{r=R_i} = D \ln R_i + Q_{4i} + \sum_m (C_{4i} + D_{4i} G_4) \cos[F_m(\alpha + b_{oa} / 2 - \alpha_i)] \quad (111)$$

According to vector potential continuation:

$$A_{z4i} \Big|_{r=R_i} = A_i \quad \text{for} \quad \alpha_i - b_{oa} / 2 \leq \alpha \leq \alpha_i + b_{oa} / 2 \quad (112)$$

it can be obtained that:

$$Q_{3i} = Q_{4i} + D \ln R_i - \mu_0 J_{i0} (2R_{sb}^2 \ln R_i - R_i^2) / 4 - \sum_n A_{3in} \zeta_0 \quad (113)$$

for the non-overlapping winding and

$$Q_{3i} = Q_{4i} + D \ln R_i - \sum_n A_{3in} \zeta_0 - \mu_0 \left[J_{i1} (R_{sm}^2 \ln R_i - R_i^2 / 2) + J_{i2} (R_{sb}^2 - R_{sm}^2) \ln R_i \right] / 2 \quad (114)$$

for the overlapping winding, and

$$C_{4i} + D_{4i} G_4 = \sum_n A_{3in} \zeta \quad (115)$$

E. Interface between Slot Opening and Air-gap

The circumferential component of the flux density along the stator bore within the slot opening can be obtained from (57) as:

$$B_{4i\alpha} \Big|_{r=R_i} = B_{i\alpha 0} + \sum_m B_{i\alpha m} \cos[F_m(\alpha + b_{oa} / 2 - \alpha_i)] \quad (116)$$

where

$$B_{i\alpha 0} = -D / R_s \quad (117)$$

$$B_{i\alpha m} = -F_m (C_{4i} G_4 - D_{4i}) / R_s \quad (118)$$

The circumferential component of the flux density along the stator bore outside the slot opening is zero since the stator core material is infinitely permeable. The circumferential component flux density along the stator bore can be expanded into Fourier series:

$$B_{s\alpha} = \sum_k [C_s \cos(k\alpha) + D_s \sin(k\alpha)] \quad (119)$$

where

$$C_s = \sum_i \sum_m B_{i\alpha m} \eta_i + \sum_i B_{i\alpha 0} \eta_{i0} \quad (120)$$

$$D_s = \sum_i \sum_m B_{i\alpha m} \xi_i + \sum_i B_{i\alpha 0} \xi_{i0} \quad (121)$$

where

$$\eta_i(m, k) = -k / \pi / (F_m^2 - k^2) \left[\cos(m\pi) \sin(k\alpha_i + kb_{oa} / 2) - \sin(k\alpha_i - kb_{oa} / 2) \right] \quad (122)$$

$$\xi_i(m, k) = k / \pi / (F_m^2 - k^2) \cdot [\cos(m\pi) \cos(k\alpha_i + kb_{oa}/2) - \cos(k\alpha_i - kb_{oa}/2)] \quad (123)$$

$$\eta_{i0}(k) = 2 \sin(kb_{oa}/2) \cos(k\alpha_i) / (k\pi) \quad (124)$$

$$\xi_{i0}(k) = 2 \sin(kb_{oa}/2) \sin(k\alpha_i) / (k\pi) \quad (125)$$

The circumferential component of the flux density along the stator bore can also be given as:

$$B_{s\alpha} = B_{2\alpha} \Big|_{r=R_s} = -\frac{1}{R_s} \sum_k k [(A_2 - B_2 G_2) \cos(k\alpha) + (C_2 - D_2 G_2) \sin(k\alpha)] \quad (126)$$

According to (119) and (126), it can be obtained that:

$$\begin{cases} -kA_2 + kG_2 B_2 = R_s C_s \\ -kC_2 + kG_2 D_2 = R_s D_s \end{cases} \quad (127)$$

The vector potential distribution along the stator bore can be given as:

$$A_s = A_{z2} \Big|_{r=R_s} = \sum_k [A_{2c} \cos(k\alpha) + A_{2s} \sin(k\alpha)] \quad (128)$$

where

$$A_{2c} = A_2 + B_2 G_2 \quad (129)$$

$$A_{2s} = C_2 + D_2 G_2 \quad (130)$$

The above expression can be expanded into Fourier series over slot opening:

$$A_s = \sum_m A_{oi} \cos[F_m(\alpha + b_{oa}/2 - \alpha_i)] + A_{oi0} \quad (131)$$

for $\alpha_i - b_{oa}/2 \leq \alpha \leq \alpha_i + b_{oa}/2$, where

$$A_{oi0} = \sum_k (A_{2c} \sigma_{i0} + A_{2s} \tau_{i0}) \quad (132)$$

$$A_{oi} = \sum_k (A_{2c} \sigma_i + A_{2s} \tau_i) \quad (133)$$

where

$$\sigma_{i0}(k) = (\pi / b_{oa}) \eta_{i0}(k) \quad (134)$$

$$\tau_{i0}(k) = (\pi / b_{oa}) \xi_{i0}(k) \quad (135)$$

$$\sigma_i(m, k) = (2\pi / b_{oa}) \eta_i(m, k) \quad (136)$$

$$\tau_i(m, k) = (2\pi / b_{oa}) \xi_i(m, k) \quad (137)$$

The vector potential distribution along the stator bore within the slot opening can also be expressed by:

$$A_{z4} \Big|_{r=R_s} = D \ln R_s + Q_{4i} + \sum_m (C_{4i} G_4 + D_{4i}) \cos[F_m(\alpha + b_{oa}/2 - \alpha_i)] \quad (138)$$

According to vector potential continuation:

$$A_{z4} \Big|_{r=R_s} = A_s \quad \text{for} \quad \alpha_i - b_{oa}/2 \leq \alpha \leq \alpha_i + b_{oa}/2 \quad (139)$$

it can be obtained that:

$$Q_{4i} = \sum_k (A_{2c} \sigma_{i0} + A_{2s} \tau_{i0}) - D \ln R_s \quad (140)$$

$$C_{4i} G_4 + D_{4i} = \sum_k (A_{2c} \sigma_i + A_{2s} \tau_i) \quad (141)$$

Combining (76)-(77), (79)-(80), (97), (115), (127) and (141), the unknowns in the vector potential expressions can be predicted.

ACKNOWLEDGMENT

This work is financially supported by the Engineering and Physics Science Research Council, UK, Ref. EP/F016506/1., and Motor Design Ltd under the Motor-CAD/FLUX Partnership Scheme.

REFERENCES

- [1] B. Ackermann and R. Sottek, "Analytical modeling of the cogging torque in permanent magnet motors," *Electrical Engineering*, vol. 78, no. 2, pp. 117-125, 1995.
- [2] Z. J. Liu and J. T. Li, "Analytical solution of air-gap field in permanent-magnet motors taking into account the effect of pole transition over slots," *IEEE Trans. Magn.*, vol. 43, no. 10, pp. 3872-3883, 2007.
- [3] Z. J. Liu, J. T. Li, and Q. Jiang, "An improved analytical solution for predicting magnetic forces in permanent magnet motors," *Journal of Applied Physics*, vol. 103, no. 7, 2008.
- [4] Z. J. Liu and J. T. Li, "Accurate prediction of magnetic field and magnetic forces in permanent magnet motors using an analytical solution," *IEEE Trans. Energy Convers.*, vol. 23, no. 3, pp. 717-726, 2008.
- [5] Z. Q. Zhu, L. J. Wu, and Z. P. Xia, "An accurate subdomain model for magnetic field computation in slotted surface-mounted permanent-magnet machines," *IEEE Trans. Magn.*, vol. 46, no. 4, pp. 1100-1115, 2010.
- [6] F. Dubas and C. Espanet, "Analytical solution of the magnetic field in permanent-magnet motors taking into account slotting effect: no-load vector potential and flux density calculation," *IEEE Trans. Magn.*, vol. 45, no. 5, pp. 2097-2109, 2009.
- [7] D. Zarko, D. Ban, and T. A. Lipo, "Analytical calculation of magnetic field distribution in the slotted air gap of a surface permanent-magnet motor using complex relative air-gap permeance," *IEEE Trans. Magn.*, vol. 42, no. 7, pp. 1828-1837, 2006.
- [8] D. Zarko, D. Ban, and T. A. Lipo, "Analytical solution for cogging torque in surface permanent-magnet motors using conformal mapping," *IEEE Trans. Magn.*, vol. 44, no. 1, pp. 52-65, 2008.
- [9] L. J. Wu, Z. Q. Zhu, D. Staton, M. Popescu, and D. Hawkins, "Comparison of analytical models for predicting cogging torque in surface-mounted PM machines," in *Int. Conf. Electrical Machines*, 2010.
- [10] E. Bolte, "Analytical calculation of the two-dimensional field in the air gap and the slots of electrical machines," *IEEE Trans. Magn.*, vol. 20, no. 5, pp. 1783-1785, 1984.
- [11] A. Bellara, Y. Amara, G. Barakat, and B. Dakyo, "Two-dimensional exact analytical solution of armature reaction field in slotted surface mounted PM radial flux synchronous machines," *IEEE Trans. Magn.*, vol. 45, no. 10, pp. 4534-4538, 2009.
- [12] L. J. Wu, Z. Q. Zhu, D. Staton, M. Popescu, and D. Hawkins, "An improved subdomain model for predicting magnetic field of surface-mounted permanent magnet machines accounting for tooth-tips," *Submitted to IEEE Trans. Magn.*, 2010.
- [13] L. J. Wu, Z. Q. Zhu, D. Staton, M. Popescu, and D. Hawkins, "Subdomain model for predicting armature reaction field of surface-mounted permanent magnet machines accounting for tooth-tips," *Submitted to IEEE Trans. Magn.*, 2010.
- [14] Z. Q. Zhu and D. Howe, "Instantaneous magnetic field distribution in brushless permanent magnet dc motors. Part III: Effect of stator slotting," *IEEE Trans. Magn.*, vol. 29, no. 1, pp. 143-151, 1993.
- [15] K. H. Kim, D. J. Sim, and J. S. Won, "Analysis of skew effects on cogging torque and BEMF for BLDCM," in *Conf. Record of the 1991 IEEE Ind. Appl. Society Annual Meeting*, 1991, pp. 191-197 vol.1.
- [16] A. B. Proca, A. Keyhani, A. El-Antably, L. Wenzhe, and D. Min, "Analytical model for permanent magnet motors with surface mounted magnets," *IEEE Trans. Energy Convers.*, vol. 18, no. 3, pp. 386-391, 2003.
- [17] P. Kumar and P. Bauer, "Improved analytical model of a permanent-magnet brushless DC motor," *IEEE Trans. Magn.*, vol. 44, no. 10, pp. 2299-2309, 2008.
- [18] D. Ishak and A. H. A. Hassan, "Analytical modeling of permanent magnet excited brushed DC motor for low-cost applications," in *5th Int. Symp. Mechatronics and Its Appl.*, 2008, pp. 1-5.
- [19] K. Boughrara, D. Zarko, R. Ibtouen, O. Touhami, and A. Rezzoug, "Magnetic field analysis of inset and surface-mounted permanent-magnet

- synchronous motors using Schwarz-Christoffel transformation," *IEEE Trans. Magn.*, vol. 45, no. 8, pp. 3166-3178, 2009.
- [20] Z. Q. Zhu, K. Ng, N. Schofield, and D. Howe, "Analytical prediction of rotor eddy current loss in brushless machines equipped with surface-mounted permanent magnets. II. Accounting for eddy current reaction field," in *Proc. the Fifth Int. Conf. Electr. Machines and Syst.*, 2001, pp. 810-813 vol.2.
- [21] L. J. Wu, Z. Q. Zhu, D. Staton, M. Popescu, and D. Hawkins, "Combined complex permeance and sub-domain model for analytical predicting electromagnetic performance of surface-mounted PM machines," in *IET Int.Conf. Power Electronics, Machines and Drives*, Brighton, UK, 2010, pp. 1-6.
- [22] L. J. Wu, Z. Q. Zhu, D. Staton, M. Popescu, and D. Hawkins, "Comparison of analytical models for predicting electromagnetic performance in surface-mounted permanent magnet machines," in *IEEE Vehicle Power and Propulsion Conf.*, 2010.
- [23] Z. Q. Zhu, D. Howe, and J. K. Mitchell, "Magnetic field analysis and inductances of brushless DC machines with surface-mounted magnets and non-overlapping stator windings," *IEEE Trans. Magn.*, vol. 31, no. 3, pp. 2115-2118, 1995.
- [24] T. J. E. Miller, *Brushless permanent-magnet and reluctance motor drives*: Oxford Science Publications, 1993.
- [25] R. Qu and T. A. Lipo, "General closed-form analytical expressions of air-gap inductances for surface-mounted permanent magnet and induction machines," in *IEEE Int.Electric Machines and Drives Conf.*, 2003, pp. 443-448 vol.1.
- [26] A. M. El-Refaie, Z. Q. Zhu, T. M. Jahns, and D. Howe, "Winding Inductances of fractional slot surface-mounted permanent magnet brushless machines," in *IEEE Ind. Appl. Soc. Annu. Meeting*, 2008, pp. 1-8.
- [27] K. Atallah, Z. Q. Zhu, and D. Howe, "Armature reaction field and winding inductances of slotless permanent-magnet brushless machines," *IEEE Trans. Magn.*, vol. 34, no. 5, pp. 3737-3744, 1998.
- [28] Z. Q. Zhu, D. Howe, and T. S. Birch, "Calculation of winding inductances of brushless motors with surface-mounted permanent magnets," in *Int.Conf. Electrical Machines*, Paris, 1994, pp. pp. 327-332.
- [29] Z. Q. Zhu and D. Howe, "Winding inductances of brushless machines with surface-mounted magnets," in *IEEE Int.Electric Machines and Drives Conf.Record*, 1997, pp. WB2/2.1-WB2/2.3.
- [30] T. J. E. Miller, M. I. McGilp, D. A. Staton, and J. J. Bremner, "Calculation of inductance in permanent-magnet DC motors," *IEE Proceedings - Electric Power Appl.*, vol. 146, no. 2, pp. 129-137, 1999.
- [31] J. Wang, W. Wang, K. Atallah, and D. Howe, "Demagnetization assessment for three-phase tubular brushless permanent-magnet machines," *IEEE Trans. Magn.*, vol. 44, no. 9, pp. 2195-2203, 2008.
- [32] K. J. Binns, P. J. Lawrenson, and C. W. Trowbridge, *The analytical and numerical solution of electric and magnetic fields*: John Wiley & Sons Ltd, 1992.
- [33] J. De La Ree and N. Boules, "Torque production in permanent-magnet synchronous motors," *IEEE Trans. Ind. Appl.*, vol. 25, no. 1, pp. 107-112, 1989.
- [34] L. Zhu, S. Z. Jiang, Z. Q. Zhu, and C. C. Chan, "Analytical methods for minimizing cogging torque in permanent-magnet machines," *IEEE Trans. Magn.*, vol. 45, no. 4, pp. 2023-2031, 2009.
- [35] Z. Q. Zhu and D. Howe, "Analytical prediction of the cogging torque in radial-field permanent magnet brushless motors," *IEEE Trans. Magn.*, vol. 28, no. 2, pp. 1371-1374, 1992.